Article ID: 1006-8775(2022) 03-0326-17

Research on the Application of the Radiative Transfer Model Based on Deep Neural Network in One-dimensional Variational Algorithm

HE Qiu-rui (贺秋瑞)[1, 2], ZHANG Rui-ling (张瑞玲)[1], LI Jiao-yang (李骄阳)[3], WANG Zhen-zhan (王振占)[2]
(1. School of Information Technology, Luoyang Normal University, Luoyang, Henan 471934 China;
2. Key Laboratory of Microwave Remote Sensing, National Space Science Center, Chinese Academy of Sciences, Beijing 100190 China; 3. Department of Electrical and Computer Engineering, Michigan State University, East Lansing, MI 48824 USA)

Abstract: As a typical physical retrieval algorithm for retrieving atmospheric parameters, one-dimensional variational (1DVAR) algorithm is widely used in various climate and meteorological communities and enjoys an important position in the field of microwave remote sensing. Among algorithm parameters affecting the performance of the 1DVAR algorithm, the accuracy of the microwave radiative transfer model for calculating the simulated brightness temperature is the fundamental constraint on the retrieval accuracies of the 1DVAR algorithm for retrieving atmospheric parameters. In this study, a deep neural network (DNN) is used to describe the nonlinear relationship between atmospheric parameters and satellite-based microwave radiometer observations, and a DNN-based radiative transfer model is developed and applied to the 1DVAR algorithm to carry out retrieval experiments of the atmospheric temperature and humidity profiles. The retrieval results of the temperature and humidity profiles from the Microwave Humidity and Temperature Sounder (MWHTS) onboard the Feng-Yun-3 (FY-3) satellite show that the DNN-based radiative transfer model can obtain higher accuracy for simulating MWHTS observations than that of the operational radiative transfer model RTTOV, and also enables the 1DVAR algorithm to obtain higher retrieval accuracies of the temperature and humidity profiles. In this study, the DNN-based radiative transfer model applied to the 1DVAR algorithm can fundamentally improve the retrieval accuracies of atmospheric parameters, which may provide important reference for various applied studies in atmospheric sciences.

Key words: one-dimensional variational algorithm; radiative transfer model; deep neural network; FY-3; MWHTS; temperature and humidity profiles
CLC number: P412.27 **Document code:** A
Citation: HE Qiu-rui, ZHANG Rui-ling, LI Jiao-yang, et al. Research on the Application of the Radiative Transfer Model Based on Deep Neural Network in One-dimensional Variational Algorithm [J]. Journal of Tropical Meteorology, 2022, 28(3): 326-342, https://doi.org/10.46267/j.1006-8775.2022.025

1 INTRODUCTION

Microwave radiometers can obtain observed brightness temperatures by measuring the microwave radiation of the Earth-Atmosphere system and be applied to detect atmospheric parameters (Turner and Löhnert [1]; Zhang et al. [2]; Ebell et al. [3]). Brightness temperatures observed by microwave radiometers can be converted into atmospheric parameters, such as temperature, humidity, and precipitation, etc., by using a retrieval algorithm (Zhang et al. [4]; Li et al. [5]; Ebell et al. [6]). The retrieval algorithms for the atmospheric temperature and humidity profiles based on passive microwave observations have been developed for more than 60 years, and can be divided into two categories: statistical retrieval algorithms and physical retrieval algorithms (Polyakov et al. [7]; Tan et al. [8]).

The essence of statistical retrieval algorithms is to establish a statistical retrieval model between the atmospheric parameters from historical data and corresponding observations of the microwave radiometer. The retrievals of corresponding atmospheric parameters can be obtained when new observations of the microwave radiometer are input into established statistical retrieval models (Gohil et al. [9]; Chakraborty and Maitra [10]; He et al. [11]; He et al. [12]). Linear regression algorithms, neural network algorithms, and ridge regression algorithms are all commonly used statistical retrieval algorithms.

The essence of physical retrieval algorithms is to input the initial values of atmospheric parameters to the radiative transfer model to calculate the simulated brightness temperatures by iterative process to

Submitted 2022-02-11; **Revised** 2022-05-15; **Accepted** 2022-08-15
Funding: National Natural Science Foundation of China (41901297, 41806209); Science and Technology Key Project of Henan Province (202102310017); Key Research Projects for the Universities of Henan Province (20A170013); China Postdoctoral Science Foundation (2021M693201)
Biography: HE Qiu-rui, Associate Professor, primarily undertaking research on numerical simulation and satellite meteorology.
Corresponding author: ZHANG Rui-ling, e-mail: ruilingzhang@163.com

continuously adjust the initial values, which makes the simulated brightness temperatures generated by the adjusted initial values be as close as possible to the observed brightness temperatures of the microwave radiometer. The iteration is completed when the differences between the simulated brightness temperatures calculated by the radiative transfer model and the observed brightness temperatures of the microwave radiometer meet a certain threshold, and then the final adjusted values are the retrievals of atmospheric parameters (Liu and Weng [13]; Aires et al. [14]). The physical retrieval algorithm fully considers the physical process of microwave transportation in the atmosphere and uses the optimal solution method to realize the retrieval calculation of atmospheric parameters. Currently, one-dimensional variational (1DVAR) algorithm is the most widely used physical retrieval algorithm (Boukabara et al. [15]; He et al. [16]).

At present, statistical inversion algorithms are widely used in the field of microwave remote sensing of the atmosphere because they do not involve any physical concept, operate easily, are fast in the calculation, and have high retrieval accuracy, etc. Meanwhile, with the development of deep neural networks (DNN), their powerful nonlinear mapping capability has led to the unprecedented development of statistical retrieval algorithms (Blackwell and Chen [17]; He et al. [18]). However, the disadvantages of statistical retrieval algorithms are also obvious, such as high dependence of the algorithm performance on the representativeness of the historical dataset, poor retrieval accuracy in extreme weather conditions, the dependence of empirical algorithm parameter settings, and limitation by the local optimality of the feature learning on historical data, etc. Especially important is that the retrieval results obtained by the statistical retrieval methods may be difficult to be interpreted from a physical point of view (He et al. [11]). Therefore, it is still necessary to rely on physical retrieval algorithms to fundamentally improve the retrieval accuracy of atmospheric parameters. This is also the reason why physical retrieval algorithms play an irreplaceable position in the field of microwave remote sensing of the atmosphere, although the computational efficiencies of physical inversion algorithms are relatively low, and a large number of parameter settings are required before retrieval.

As a typical representative of physical retrieval algorithms, 1DVAR algorithm is still the core algorithm for retrieving atmospheric parameters in meteorological and climate communities (Liu and Weng [13]; Aires et al. [14]; Rosenkranz [19]; Ishimoto [20]). Moreover, 1DVAR and the numerical weather prediction (NWP) radiance assimilation based on the variational approach are mathematically similar concepts sharing a number of common characteristics, such as minimizing a similar cost function, both need to set representative and accurate covariance matrices and mean backgrounds, simulating observations by similar radiative transfer model, etc. (Boukabara et al. [15]). Therefore, carrying out the study of 1DVAR algorithm and then improving the retrieval accuracies of atmospheric parameters based on 1DVAR algorithm is of great significance for various theoretical and applied research in atmospheric science, and provides important reference for NWP radiance assimilation systems.

For the 1DVAR algorithm, there are many factors that affect its algorithm performance, such as the setting of the initial state of atmospheric parameters, the calculation of the mean background and the covariance matrices, the accuracy of the radiative transfer model for simulation, and the bias correction for observations. However, the computational accuracy of the radiative transfer model for simulating observations is an important factor limiting the performance of the 1DVAR algorithm (Rodgers [21]; Susskind et al. [22]). Currently, the radiative transfer models used in the 1DVAR algorithm are all physical models developed by various remote sensing scientific communities, such as Radiative Transfer for TOVS (RTTOV) developed by the European Centre for Medium-Range Weather Forecasts (ECMWF), Community Radiative Transfer Model (CRTM) developed by the Joint Center for Data Assimilation (JCDA) of the United States, Atmospheric Radiative Transfer Simulator (ARTS) developed jointly by Hamburg University and Chalmers University (Saunders et al. [23]; Liu and Boukabara [24]; Buehler et al. [25]; Eriksson et al. [26]).

The physical-based radiative transfer model takes the radiative transfer equation as the physical basis to describe the transfer process of the microwave in the atmosphere, establishes a nonlinear model between the atmospheric parameters and the observed brightness temperatures of the microwave radiometer, and realizes the purpose of outputting the simulated brightness temperatures of the microwave radiometer by inputting the atmospheric parameters to the radiative transfer model. However, the establishment of the radiative transfer model requires an accurate description of the physical process of microwave transmission in the atmosphere, which is difficult to be modeled under some weather conditions, especially under the cloudy and rainy sky (Elachi and Zyl [27]). Therefore, the accuracy of the physical-based radiative transfer model for the simulated brightness temperature has been restricted. Even so, the existing physical-based radiative transfer models are widely used in various atmospheric applications and scenarios. They have comparable accuracy in describing the physical processes of microwave transmission in the atmosphere, and in turn, comparable accuracy in simulating the observations of the microwave radiometer.

From the perspective of improving the 1DVAR algorithm, it is expected to further improve the accuracies of the 1DVAR algorithm for retrieving the

atmospheric parameters if a radiative transfer model with higher accuracy for simulating the observations is applied to the 1DVAR algorithm. In recent years, deep neural network (DNN) has been developed rapidly due to its powerful nonlinear mapping capability, and has been widely used in the field of microwave remote sensing (He et al. [11]; Yan et al. [28]). In this study, DNN is used to describe the nonlinear relationship between atmospheric parameters and microwave observations, and a DNN-based radiative transfer model is established. Then, the DNN-based radiative transfer model is applied to the 1DVAR algorithm, and the 1DVAR retrieval system is built to carry out a retrieval study of the atmospheric temperature and humidity profiles based on the observations of MWHTS onboard Feng-Yun-3D (FY-3D) satellite.

The structure of this paper is organized as follows. Section 2 introduces MWHTS characteristics and the atmospheric data used in this study. Section 3 describes the establishment of the DNN-based radiative transfer model. The detailed description of the 1DVAR algorithm and the establishment of the 1DVAR retrieval system are presented in Section 4. The experimental design of this study is elaborated in Section 5, followed by the experimental results presented in Section 6. Finally, the conclusions of this study are given in Section 7.

2 DATA DESCRIPTION

2.1 *MWHTS observations*

In this study, the observed brightness temperatures of Microwave Humidity and Temperature Sounder (MWHTS) onboard the FY-3D satellite are used to carry out the retrieval study of the atmospheric temperature and humidity profiles. MWHTS is an important payload onboard Feng-Yun-3C (FY-3C) and FY-3D satellites. MWHTS has a total of 15 channels in the range of 89 GHz to 183 GHz, which can realize the simultaneous detection of atmospheric temperature and humidity. MWHTS has eight temperature sounding channels set in the 118 GHz band to provide the temperature information from the surface to about 30 hPa. MWHTS contains five humidity sounding channels set in the 183 GHz band, which are mainly used to detect the water vapor distribution in the troposphere. In addition, MWHTS also includes two window channels set at 89 GHz and 150 GHz, respectively, which can provide surface information such as surface temperature, surface humidity, pressure, etc. As a total power microwave radiometer, MWHTS performs the cross-track scanning along the orbit with the angle of 53.35° from the nadir to inspect 98 nominal fields of view (FOVs) in each scan line, which is corresponding to the scanning of a swath of 2645 km in 2.667 s (Guo et al. [29]; Wang et al. [30]; He et al. [31]; Carminati and Migliorini [32]). Table 1 lists major channel characteristics of MWHTS. Level 1b brightness temperatures of MWHTS onboard FY-3D satellite are used in this study, which are available from the National Satellite Meteorological Center (NSMC) (http://satellite.nsmc.org.cn).

2.2 *Atmospheric data*

In this study, the atmospheric parameters from the ERA-Interim reanalysis dataset provided by ECMWF are used to develop and validate the DNN-based radiative transfer model, generate parameters for the retrieval algorithm, and validate the performance of the retrieval system. ERA-Interim is a global atmospheric reanalysis describing the recent history of the atmosphere, land surface, and oceans, produced by the

Table 1. Channel characteristics of MWHTS.

Channel	Frequency (GHz)	Sensitivity (K)	In-flight sensitivity (K)	Calibration accuracy (K)	Peak WF height (hPa)
1	89.0	1.0	0.23	1.3	surface
2	118.75±0.08	3.6	1.62	2.0	30
3	118.75±0.2	2.0	0.75	2.0	50
4	118.75±0.3	1.6	0.59	2.0	100
5	118.75±0.8	1.6	0.65	2.0	250
6	118.75±1.1	1.6	0.52	2.0	350
7	118.75±2.5	1.6	0.49	2.0	surface
8	118.75±3.0	1.0	0.27	2.0	surface
9	118.75±5.0	1.0	0.27	2.0	surface
10	150.0	1.0	0.34	1.3	surface
11	183.31±1.0	1.0	0.47	1.3	300
12	183.31±1.8	1.0	0.34	1.3	400
13	183.31±3.0	1.0	0.30	1.3	500
14	183.31±4.5	1.0	0.22	1.3	700
15	183.31±7.0	1.0	0.27	1.3	800

forecast model and data assimilation system. ERA-Interim is very popular and is used for monitoring climate change, validating the retrieval algorithm, and commercial applications. For a detailed documentation of the ERA-Interim Archive, please refer to Dee et al. [33]. In this study, the profile parameters used in ERA-Interim include temperature, specific humidity, cloud cover, cloud liquid water, and cloud ice water, which have a total of 37 pressure levels unevenly distributed from 1000 to 1 hPa. The surface parameters used in ERA-Interim include 2 m temperature, 2 m dewpoint temperature, surface pressure, skin temperature, 10 m *u* wind component, and 10 m *v* wind component. The profile parameters and the surface parameters are used to build the atmospheric dataset with a space resolution of $0.5° \times 0.5°$ and a temporal resolution of 6 h (i. e., with data available at 0000 UTC, 0600 UTC, 1200 UTC, and 1800 UTC).

2.3 *Data preprocessing*

In this study, MWHTS brightness temperatures from the ocean area of 25° N−45° N and 160° E−220° E from 1 January 2019 to 30 June 2019 are selected to retrieve the atmospheric temperature and humidity profiles. According to the research purpose of this paper, the following pre-processing is required for MWHTS brightness temperatures and the atmospheric dataset. MWHTS brightness temperatures are collocated with the atmospheric parameters in the atmospheric dataset with the criteria that their time difference is less than 10 min and the absolute distances between their positions (latitude and longitude) are less than 0.1 °. Thus, 510500 collocated samples can be obtained. Since DNN is used in this study to describe the relationship between atmospheric parameters and MWHTS observed brightness temperatures, the training, and validation of DNN are performed. Moreover, the parameters of the 1DVAR algorithm need to be set, and the validation of the algorithm performance is conducted in the study. Therefore, the collocated samples from 1 January 2019 to 31 May 2019 from the analysis dataset with 425911 collocated samples are used to develop the DNN-based radiative transfer model and set the parameters of the 1DVAR algorithm. The collocated samples from 1 June 2019 to 30 June 2019 are taken as the testing dataset with 84589 collocated samples for validating the DNN-based radiative transfer model and the 1DVAR algorithm.

3 DNN−BASED RADIATIVE TRANSFER MODEL

The key problems studied in the field of microwave remote sensing can be divided into two categories: one is the retrieval problem and the other is the forward problem (Ulaby et al. [34]). The so-called retrieval problem is the conversion from microwave observations into atmospheric parameters. In recent years, neural networks have been widely used in the retrieval of the atmospheric parameters using passive microwave observations due to their powerful nonlinear mapping capability. Typically, for retrieving the atmospheric parameters based on neural networks, the microwave observations are used as the input and the specific atmospheric parameters collocating the microwave observations are used as the output to train the neural network. When new microwave observations are input to the trained neural network model for prediction, the predicted values for specific atmospheric parameters corresponding to the new microwave observations are obtained, i. e., the retrievals of specific atmospheric parameters (Zhou and Grasstotti [35]; Li et al. [36]; Tan et al. [37]). The transformation from microwave observations to atmospheric parameters is achieved since neural network can describe the nonlinear relationship between microwave observations and atmospheric parameters.

The transformation from atmospheric parameters to microwave observations is the forward problem in the field of microwave remote sensing (Rodgers [38]). At present, almost all the solutions to the forward problem are modeling the interaction between microwave and atmospheric components from a physical perspective and obtaining physical-based radiative transfer models, such as RTTOV, CRTM, ARTS, etc. In essence, the physical-based radiative transfer model is a description of the nonlinear relationship between atmospheric parameters and microwave observations (Ulaby et al. [34]). However, inspired by the application of neural networks to the retrieval problem, the nonlinear relationship between atmospheric parameters and the microwave observations described in the physical-based radiative transfer model can also be described using neural networks. The neural network is trained by taking atmospheric parameters as the input and the microwave observations collocating atmospheric parameters as the output. When the new atmospheric parameters are fed into the trained neural network for prediction, the predicted values of the microwave observations corresponding to the new atmospheric parameters are obtained, i. e., the simulated values of the microwave observations. This is also the basic procedure of building a DNN-based radiative transfer model in this study.

Rather than using the traditional radiative transfer model which models the transformation of microwave in the atmosphere from a physical perspective, this study uses DNN to describe the nonlinear relationship between atmospheric parameters and microwave observations, and then builds a DNN-based radiative transfer model. This section presents the structure and parameter configuration of the developed DNN, and describes the method of building the DNN-based radiative transfer model.

3.1 *DNN algorithm*

Compared with shallow neural networks, deep neural networks have better nonlinear computational

power due to more hidden layers and more neurons in the hidden layers, and therefore can achieve better prediction performance (Lecun et al. [39]; Lee et al. [40]). According to the objectives and requirements for this study, a four-layer deep neural network is developed, which contains an input layer for inputting the input samples, an output layer for outputting the output samples, and two hidden layers for nonlinear computation to describe the nonlinear relationship between input samples and output samples. The numbers of neurons in the input layer and the output layer are determined based on the input samples and the output samples, while the numbers of neurons in the two hidden layers need to be set by performing a large number of test experiments in order to obtain the optimal prediction performance.

In the process of optimizing the parameter configuration of the DNN through extensive test experiments, a training dataset is used to train the DNN and a testing dataset is used to evaluate the predictions of the trained DNN, where the Root Mean Square Error (RMSE) between the predicted values of the trained DNN and the corresponding true values in the testing dataset are used as an indicator to evaluate the performance of the DNN. The Rectified Linear Unit (ReLU) is chosen as the activation function in the hidden layers of the DNN due to its superiority over sigmoid and Leaky ReLU in overcoming the problems of saturation and vanishing gradients, and obtaining the highest prediction accuracy (Yan et al. [28]). It is also important to note that setting too few epochs during training may result in obtaining an underfit model, and setting too many epochs may result in overfitting. To deal with this problem, an underfit model is avoided by setting a sufficiently large number of epochs, and early stopping is chosen to prevent overfitting (Srivastava et al. [41]). Early stopping splits the training dataset and uses a subset (20%) as a validation dataset to monitor the performance of DNN in the training. The training will be terminated if the loss on the validation dataset does not change over a given number of epochs (i. e., patience). Based on the requirements of this study for the application of nonlinear models, the maximum number of epochs and the patience for the designed DNN is 3000 and 100, respectively.

3.2 *DNN-based radiative transfer model*

According to the configuration of the DNN in Section 3.1, the atmospheric parameters and satellite viewing angles in the analysis dataset built in Section 2.3 are used as the input samples, and the observed brightness temperatures of all 15 channels of MWHTS in the analysis dataset are used as the output samples to train the DNN; thus, the number of neurons in the input layer is 192 and the number of neurons in the output layer is 15. A set of experiments are carried out to test the effect of different numbers of neurons in the hidden layers on the performance of the DNN. When the numbers of neurons in the hidden layers are both set to be 512, the optimal prediction performance of the DNN can be obtained, and a DNN-based radiative transfer model can be established. The atmospheric parameters and satellite viewing angles in the testing dataset are fed into the DNN-based radiative transfer model to obtain the DNN-based simulated brightness temperatures of MWHTS. The accuracy of the DNN-based radiative transfer model can be evaluated using MWHTS observed brightness temperatures in the testing dataset. The schematic diagram for building the DNN-based radiative transfer model is shown in Fig. 1.

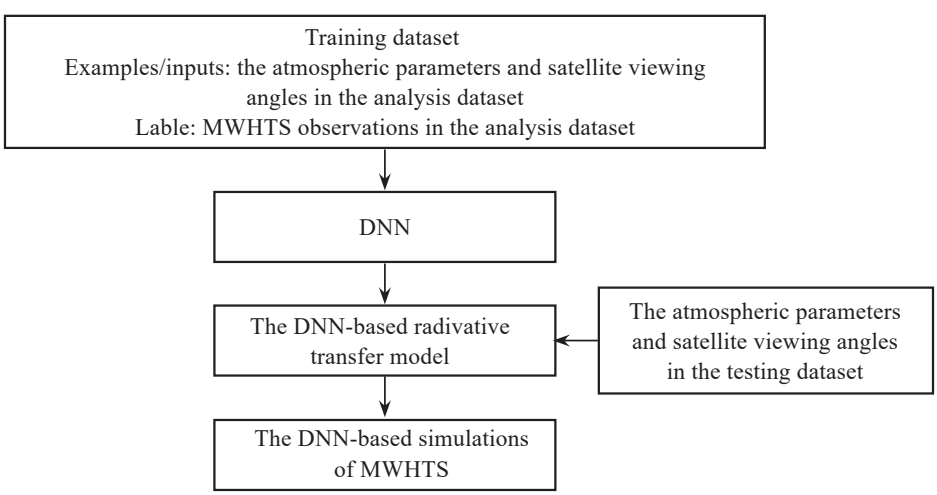

Figure 1. The schematic diagram for building the DNN-based radiative transfer model.

4 1DVAR RETRIEVAL SYSTEM

4.1 *1DVAR algorithm*

As a typical physical retrieval algorithm, the 1DVAR algorithm inputs the initial state variable into the radiative transfer model to calculate the simulated brightness temperature and compares it with the observed brightness temperature, and then adjusts the

initial state variable by using an iterative algorithm, with the aim of fitting the simulated brightness temperature produced by the adjusted initial state variable and the observed brightness temperature until the difference between the simulated brightness temperature and the observed brightness temperatures meets a set threshold, at which point the adjusted initial state variable is the retrieval value corresponding to the observed brightness temperature. The 1DVAR algorithm consists of two main parts. One is the radiative transfer model, which usually chooses the operational radiative transfer model, such as RTTOV, CRTM, and ARTS. The other is the cost function, which can be expressed as (Boukabara et al. [15]),

$$\zeta = \frac{1}{2}(S-S_a)^{\mathrm{T}}\mathrm{C}_{\mathrm{SS}}^{-1}(S-S_a)+\frac{1}{2}[\mathrm{f}(S)-\widetilde{R}]^{\mathrm{T}}\mathrm{C}_{\psi\psi}^{-1}[\mathrm{f}(S)-\widetilde{R}] \quad (1)$$

where $\widetilde{R}$ is the observed brightness temperature, $C_{\psi\psi}$ is the observation error covariance matrix, S_a is the background state variable, C_{SS} is the background covariance matrix, f(S) represents the radiative transfer model that simulates the observed brightness temperature at the atmospheric state variable S, and T represents the matrix transpose. Provided that the errors in the observations are neither biased nor correlated, Gaussian distribution, the optimal estimate of the atmospheric state variable, can be obtained by minimizing the cost function,

$$S_{n+1} = S_a + C_{\mathrm{SS}}K_n^T[K_nC_{\mathrm{SS}}K_n^T+C_{\psi\psi}]^{-1}[\widetilde{R}-\mathrm{f}(S)]-K_n(S_a-S_n)] \quad (2)$$

where $K=\nabla_S\mathrm{f}(S)$ is the Jacobians for S, and represents the derivative of the simulated brightness temperature with respect to S, n is the iteration index, S_1 is the initial state variable, and S_{n+1} is the optimal estimate of the atmospheric state variable, i. e., the retrieval of the specific atmospheric parameter. Equation 2 shows that the parameters of the 1DVAR algorithm contain the background state variable, the initial state variable, the background covariance matrix, the radiative transfer model, the bias between the observed brightness temperature and the simulated brightness temperature (observation bias), and the observation error covariance matrix, all of which have direct impacts on the retrieval accuracy of the 1DVAR algorithm. The 1DVAR retrieval system can be established by setting these parameters of the 1DVAR algorithm.

4.2 *1DVAR retrieval system*

4.2.1 A PRIORI INFORMATION

Among the many parameters of the 1DVAR algorithm, the background covariance matrix, the background state variable, and the initial state variable are collectively referred to as the prior information for the 1DVAR algorithm. The essence of the 1DVAR algorithm is to find the inverse of the radiative transfer equation, and to find the optimal solution among an infinite number of solutions through an iterative algorithm. The role of the prior information is to restrict the optimal solution to the practical atmospheric state, and therefore crucial, as it directly determines whether an optimal solution exists and the accuracy of the optimal solution (Sahoo et al. [42]).

The background covariance matrix describes the statistical variability characteristics of the atmospheric state variables at a specific time and over a specific space location, and is typically generated using historical atmospheric datasets, such as Radiosonde Observation (RAOB) data, and reanalysis data. The elements and the correlations between the elements in the background covariance matrix are directly related to the statistical characteristics of the atmospheric state, and therefore a more representative background covariance matrix will be obtained by taking into account factors such as time, place, and season in calculating the background covariance matrix. Furthermore, the data volume of the historical data used to calculate the background covariance matrix has an important influence on the retrieval accuracy of the 1DVAR algorithm. The statistical characteristics of the background covariance matrix calculated using a larger volume of historical data are more pronounced and will result in a higher retrieval accuracy of the 1DVAR algorithm, but are not favorable for case studies in specific weather conditions. For case studies in specific atmospheric states, the background covariance matrix is usually calculated using historical data for a short period before and after microwave observations. This paper focuses on retrieving the temperature and humidity profiles over specific regions of the ocean, and uses the temperature and humidity profiles from the analysis dataset built in Section 2.3 to generate the background covariance matrix. The background covariance matrix is expressed as (Boukabara et al. [15]),

$$\sigma_{ij}^2 = \frac{1}{N}\sum_{i=1}^{N}\sum_{j=1}^{N}(S_i-\overline{S}_i)\times(S_j-\overline{S}_j) \quad (3)$$

where σ_{ij}^2 is one of the elements of the matrix corresponding to row i and column j. $\overline{S}$ is the mean value along the row or along the column, and N is the number of the temperature profiles or the humidity profiles used to calculate the matrix.

Typically, the background state variable is available from the retrieval of the statistical retrieval algorithm, the output of the numerical weather prediction model, or the average value of the climatological dataset. The output of the statistical retrieval algorithm is obtained by building a statistical model for retrieving, which in turn serves as a background state variable for the 1DVAR algorithm. This often results in high accuracy, but obviously increases the computational effort in the retrieving. Forecast data output from a numerical weather prediction model is often used as a background state variable because of its high accuracy, but its small

temporal resolution has limitations in terms of real-time atmospheric soundings. Although the mean value of the climatological dataset differs significantly from the practical atmospheric state, which can adversely affect the retrieval accuracy of the 1DVAR algorithm, it is more commonly used in theoretical studies to investigate the effect of a given algorithm parameter on the algorithm performance of the 1DVAR due to its easy accessibility and low computational effort. This paper is designed to investigate the effect of the DNN-based radiative transfer model on the retrieval performance of the 1DVAR algorithm, and therefore uses the mean temperature profiles and the mean humidity profiles from the analysis dataset built in Section 2.3 as the background profiles for the 1DVAR retrieval system.

The initial state variable is used as the initial input to get the physical iterative process started. Theoretically, the closer the initial state variable is to the true value, the faster the iterative process converges, but it does not affect the final retrieval accuracy of the 1DVAR algorithm. The methods used to obtain the background state variable can all be used to obtain the initial state variable (Srivastava et al. [41]). In this study, the mean temperature profiles and the mean humidity profiles from the analysis dataset built in Section 2.3 are also used as the initial profiles for the 1DVAR retrieval system.

4.2.2 OBSERVATION BIAS CORRECTION

The 1DVAR algorithm retrieves the atmospheric parameter using an iterative technique under the assumption that observations are unbiased and have Gaussian errors. The observation bias should be taken into account when determining the appropriate weight of observations in the 1DVAR retrieval process. Therefore, it must be quantified and removed. However, the causes of observation bias are manifold and complicated, which are related to the systematic errors in any one (but generally a combination) of the following sources: the satellite sounder (e. g., poor calibration or adverse environmental effects), the radiative transfer model (e.g., errors in the physics, or spectroscopy, or from the non-modeled atmospheric process, etc.), and errors in the atmospheric parameters from some data sources (e. g., radiosonde observations, NWP analysis, climate reanalysis, etc.) (Dee [43]; Auligne et al. [44]; Gayfulin et al. [45]). The observation bias correction scheme based on a statistical model whose calculation process is simple has been widely used in the NWP data assimilation system and the retrieval systems (Kazumori [46]; Zhu et al. [47]; Dee and Uppala [48]). Nowadays, the bias correction schemes are mainly divided into linear and nonlinear corrections, which represent the linear and nonlinear relationships between satellite observations and air mass, respectively, and the nonlinear corrections have a superior correction performance (He et al. [49]). Neural networks are widely used in observation bias correction due to their strong nonlinear mapping capability.

In our study, a DNN model is also used to correct the observation bias and the bias correction method based on DNN is developed. First, the atmospheric parameters from the testing dataset built in Section 2.3 are input to the radiative transfer model to calculate the simulated brightness temperatures. Then, input the collocated samples from 1 June 2019 to 22 June 2019 in the testing dataset from the retrieval analysis dataset with 63442 collocated samples, including the atmospheric parameters, the simulated brightness temperatures, and the observed brightness temperatures, and the remaining collocated samples in the testing dataset from the retrieval testing dataset with 21147 collocated samples.

The bias correction method based on DNN is performed as follows. The observed brightness temperatures in the retrieval analysis dataset and the observation biases (the observed brightness temperatures minus the simulated brightness temperatures) in the retrieval analysis dataset are used as the inputs and the outputs of the DNN model, respectively, to train the DNN, and then a bias correction model based on DNN is built, and the observed brightness temperatures in the retrieval testing dataset is used to be the inputs for the bias correction model based on DNN to generate the predictions of the observations bias in the retrieval testing dataset. Finally, the corrected brightness temperatures can be obtained by the observed brightness temperatures minus the predictions of the observation bias in the retrieval testing dataset. The scheme of the bias correction process is shown in Fig. 2.

4.2.3 OBSERVATION ERROR COVARIANCE MATRIX

The observation error covariance matrix is generated using the observation bias and the sensitivities of MWHTS channels measured in flight shown in Table 1. The observation error contains the observation bias and the channel sensitivity, which is usually considered to be independent of each other in the radiometer channels, so that the observation error covariance matrix can be expressed as a diagonal matrix, and the diagonal elements can be expressed as (Löhnert et al. [50])

$$r^2 = f^2 + e^2 \tag{4}$$

where r is the square roots of the diagonal elements of the observation error covariance matrix, f is the channel sensitivity measured in flight, and e is the observation bias.

4.2.4 THE JACOBIANS FOR THE RETRIEVAL PARAMETERS

Currently, Jacobian is usually calculated numerically. For the temperature profile T, the Jacobian for the temperature at the ith pressure level can be expressed as

$$K_{T,i} = T_B(T_i + 0.5) - T_B(T_i - 0.5) \tag{5}$$

where T_i denotes the temperature at the ith pressure level, and T_B is the simulated brightness temperature calculated by the radiative transfer model. $K_{T,i}$ represents the change of the simulated brightness temperature

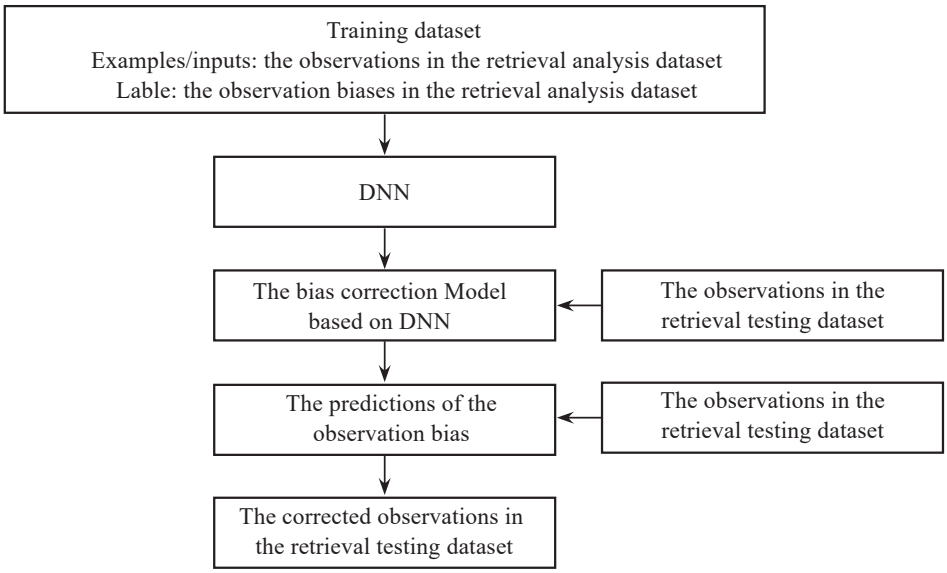

Figure 2. The schematic diagram of the bias correction based on DNN.

corresponding to each 1 K change in the temperature at the *i*th pressure level. Similarly, the Jacobian for the water vapor at the *i*th pressure level can be expressed as,

$$K_{H,i}=T_B(H_i-0.05H_i)-T_B(H_i+0.05H_i) \quad (6)$$

where H_i is the water vapor at the *i*th pressure level. $K_{H,i}$ represents the change of the simulated brightness temperature corresponding to each 10% change in the water vapor at the *i*th pressure level.

Based on the above settings of the background covariance matrix, the background profiles, the initial profiles, the observation error covariance matrix, the Jacobians for the temperature and humidity, and the correction of the observation bias for the 1DVAR algorithm using the analysis dataset, the 1DVAR retrieval system can be developed. The iteration is stopped if the relative difference of the cost function within two iterations is less than 0.01. Moreover, if the iterative times reach 10, the iteration is also stopped, and the retrieval is set to the initial profile. The overall process of building the 1DVAR retrieval system in this study is summarized in Fig. 3.

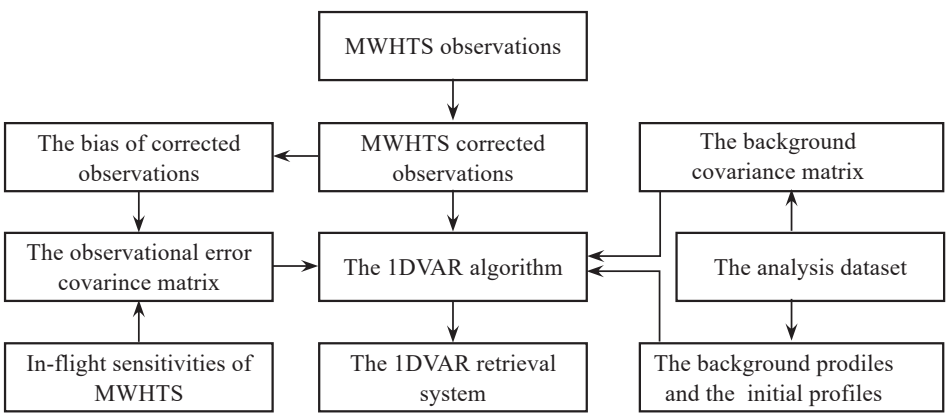

Figure 3. The schematic diagram of building the 1DVAR retrieval system.

5 EXPERIMENT DESIGN

To evaluate whether the DNN-based radiative transfer model developed in this study can improve the retrieval accuracy of the 1DVAR retrieval system when applied to it, the following three experiments are designed.

Experiment 1: Evaluation of the DNN-based radiative transfer model. The purpose of this experiment is to evaluate the accuracy of the DNN-based radiative transfer model for simulating MWHTS observed brightness temperatures. The specific experimental design is as follows.

The DNN-based radiative transfer model is built according to the procedure given in Section 3.2. The atmospheric parameters and satellite viewing angles in the testing dataset are input to the DNN-based radiative transfer model to obtain the DNN-based simulated brightness temperatures of MWHTS. For comparison, the same atmospheric parameters and satellite viewing

angles are also input to the fast radiative transfer model RTTOV v11.3 to obtain the RTTOV-based simulated brightness temperatures of MWHTS. The MWHTS observed brightness temperatures in the testing dataset are used to validate the accuracies of the two sets of simulated brightness temperatures.

Experiment 2: The observation bias correction for MWHTS. The correction of observation bias for MWHTS has a direct impact on the retrieval accuracy of the 1DVAR retrieval system. However, when the DNN-based radiative transfer model and RTTOV are applied separately to the 1DVAR retrieval system, the bias between MWHTS observed brightness temperature and the DNN-based simulated brightness temperature (DNN-based observation bias) is different from the bias between MWHTS observed brightness temperature and the RTTOV-based simulated brightness temperature (RTTOV-based observation bias), which in turn leads to different bias correction effects and different retrieval results. To compare the correction effect of the DNN-based observation bias with that of the RTTOV-based observation bias, the experiment is designed as follows.

First, the atmospheric parameters and satellite viewing angles in the retrieval analysis dataset and retrieval testing dataset established in Section 4.2.2 are input to the DNN-based radiative transfer model to obtain the DNN-based simulated brightness temperatures and to RTTOV to obtain the RTTOV-based simulated brightness temperatures. Then the collocated samples in both the retrieval analysis dataset and the retrieval testing dataset including the atmospheric parameters, the DNN-based simulated brightness temperatures, the RTTOV-based simulated brightness temperatures, and the observed brightness temperatures. Next, following the bias correction process for MWHTS observed brightness temperatures in Section 4.2.2, the DNN-based corrected brightness temperatures are obtained when the observation biases in the retrieval analysis dataset in Fig. 2 are the differences between the observed brightness temperatures minus the DNN-based simulated brightness temperatures. And when the observation biases in the retrieval analysis dataset in Fig. 2 are the differences between the observed brightness temperatures minus the RTTOV-based simulated brightness temperatures, the RTTOV-based corrected brightness temperatures can be obtained. Finally, the evaluation of the bias correction effects of the two sets of corrected brightness temperatures can be performed using the observed brightness temperatures in the retrieval testing dataset.

Experiment 3: The 1DVAR retrieval system retrieving the atmospheric temperature and humidity profiles using MWHTS observations. The purpose of this experiment is to evaluate the impact of the DNN-based radiative transfer model on the retrieval accuracies of the temperature and humidity profiles when it is applied to the 1DVAR retrieval system. The specific experimental design is as follows.

The DNN-based 1DVAR retrieval system is created when the radiative transfer model is set by the DNN-based radiative transfer model in the 1DVAR retrieval system built in Section 4.2. MWHTS observed brightness temperatures and the DNN-based corrected brightness temperatures in the retrieval testing dataset built in Experiment 2 are input to the DNN-based 1DVAR retrieval system separately to obtain the DNN-based retrieval results before and after the DNN-based observation bias correction. The correction effect of the DNN-based bias on the retrieval accuracy of the DNN-based 1DVAR retrieval system can be evaluated by comparing these two retrieval results. Similarly, the RTTOV-based 1DVAR retrieval system is created when the radiative transfer model is set to be RTTOV in the 1DVAR retrieval system. MWHTS observed brightness temperatures and the RTTOV-based corrected brightness temperatures are input to the RTTOV-based 1DVAR retrieval system separately to obtain the RTTOV-based retrieval results before and after the RTTOV-based observation bias correction. The correction effect of the RTTOV-based bias on the retrieval accuracy of 1DVAR retrieval system can be evaluated by comparing these two retrieval results.

Furthermore, by comparing the DNN-based retrieval results with the RTTOV-based retrieval results, we can validate whether the DNN-based radiative transfer model can improve the retrieval accuracies of temperature and humidity profiles when applied to the 1DVAR retrieval system compared to RTTOV.

6 EXPERIMENTAL RESULTS

This section presents the calculated results of the simulated brightness temperatures from the DNN-based radiative transfer model and RTTOV, the results of the DNN-based observation bias correction and RTTOV-based observation bias correction, and the retrieval results of the temperature and humidity profiles from the DNN-based 1DVAR retrieval system and the RTTOV-based 1DVAR retrieval system, respectively. In this study, the calculation accuracy of the radiative transfer model is evaluated using RMSE between the simulated brightness temperatures and the observed brightness temperatures in the testing dataset. The bias correction effect is evaluated using RMSE between the observed brightness temperatures and the corrected brightness temperatures in the retrieval testing dataset. Moreover, the retrieval results are evaluated using RMSE between the retrievals of the temperature and humidity profiles and the temperature and humidity profiles from the ERA-Interim reanalysis in the retrieval testing dataset.

6.1 *Calculated results of the DNN-based Radiative Transfer Model and RTTOV*

According to the design of Experiment 1 in Section 5, the atmospheric parameters and satellite viewing angles in the testing dataset are input into the DNN-

based radiative transfer model and RTTOV, respectively, to obtain 84589 sets of the DNN-based simulated brightness temperatures and 84589 sets of the RTTOV-based simulated brightness temperatures. The accuracies of these two simulated brightness temperatures are validated by using the observed brightness temperatures in the testing dataset. The comparison of the DNN-based simulated brightness temperatures and the RTTOV-based simulated brightness temperatures is shown in Fig. 4.

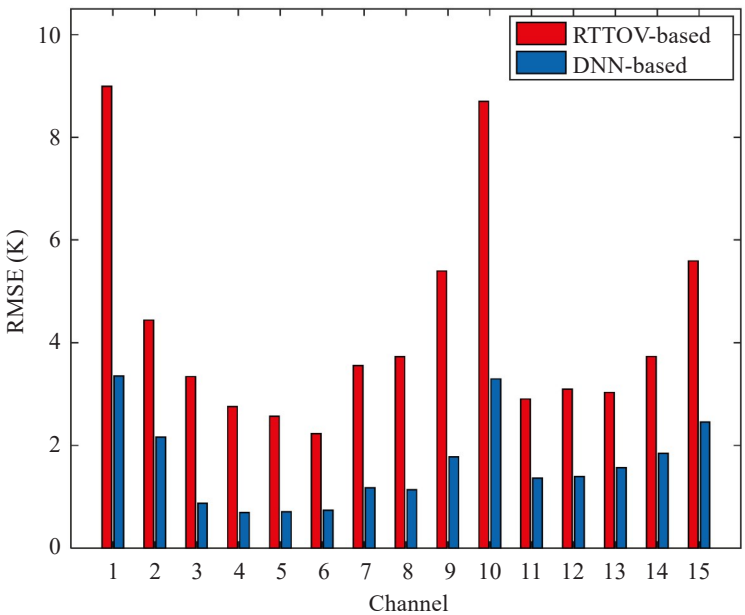

Figure 4. The comparison of MWHTS simulated brightness temperatures calculated by the DNN-based radiative transfer model with that calculated by RTTOV.

It can be seen from Fig. 4 that the accuracies of the RTTOV-based simulated brightness temperatures in window channels 1 and 10, temperature sounding channels 7-9, and humidity sounding channels 14-15 are poor, and the worst accuracy of the RTTOV-based simulated brightness temperature is in the accuracy of channel 1, which is about 9 K. The main reason is that the peak WF heights of these channels are close to the surface, and the radiations observed by these channels mainly come from the near-surface atmosphere and surface, which means the errors in the temperature, water vapor, and surface parameters can all affect the measurements of these channels. Thus, the nonlinearity between the simulated brightness temperatures and atmospheric parameters is relatively complex. The radiations observed by the temperature sounding channels 3-6 with the peak WF heights far from the surface are mainly from the atmospheric temperature, and the accuracies of the RTTOV-based simulated brightness temperature in these channels are relatively high, which are within 3 K. However, although the peak WF height of the temperature sounding channel 2 is distributed in the upper atmosphere, the accuracy of the simulated brightness temperature in channel 2 is poor, which is about 4.5 K. The reason for this may be the poor in-orbit sensitivity of channel 2 as shown in Table 1. The accuracies of the simulated brightness temperatures in the humidity sounding channels 11-13 are mainly affected by water vapor and are within 3 K.

For the DNN-based radiative transfer model, as shown in Fig. 4, the accuracies of the DNN-based simulated brightness temperatures in window channels 1 and 10 are about 3.4 K, the accuracies of the DNN-based simulated brightness temperature in temperature sounding channels 7-9 and humidity sounding channels 14-15 with peak WF heights close to the surface are within 2 K, and the accuracies of the DNN-based simulated brightness temperatures in temperature sounding channels 2-6 and humidity sounding channels 11-13 with peak WF heights far from the surface are within 2 K. Similar to the calculation results of RTTOV, the accuracy of the DNN-based simulated brightness temperatures in channel 2 is 2 K due to the poor in-orbit sensitivity.

Compared with RTTOV, the accuracies of the simulated brightness temperatures calculated by the DNN-based radiative transfer model are significantly improved in all 15 channels of MWHTS. Due to the powerful nonlinear mapping capability of DNN, for channels 1, 7-9, and 14-15 with the relatively complex relationships between the measurements and the atmospheric parameters, the accuracies of the simulated brightness temperatures calculated by the DNN-based radiative transfer model in these channels have great improvements. Especially for window channel 10, the improvement of the simulation accuracy is the largest at 5.6 K. Compared with RTTOV, the improvements in accuracies of the simulated brightness temperatures

calculated by the DNN-based radiative transfer model are all above 1.5 K in channels 2-6 and 11-13 with peak WF heights far from the surface. By comparison, it can be found that the DNN-based radiative transfer model can obtain higher accuracy than RTTOV for simulating MWHTS observed brightness temperatures.

6.2 *Correction results of the observation bias*

Following the design of Experiment 2 in Section 5, the observed brightness temperatures in the retrieval testing dataset are corrected for the observation biases, and 21147 sets of the DNN-based corrected brightness temperatures and 21147 sets of the RTTOV-based corrected brightness temperatures are obtained, respectively. The correction effects of the RTTOV-based observation biases and the DNN-based observation biases are evaluated using the observed brightness temperatures in the retrieval testing dataset, as shown in Fig. 5 and Fig. 6, respectively. Moreover, RMSEs between the RTTOV-based corrected brightness temperatures and the RTTOV-based simulated brightness temperatures, and RMSEs between the DNN-based corrected brightness temperatures and the DNN-based simulated brightness temperatures are summarized in Table 2.

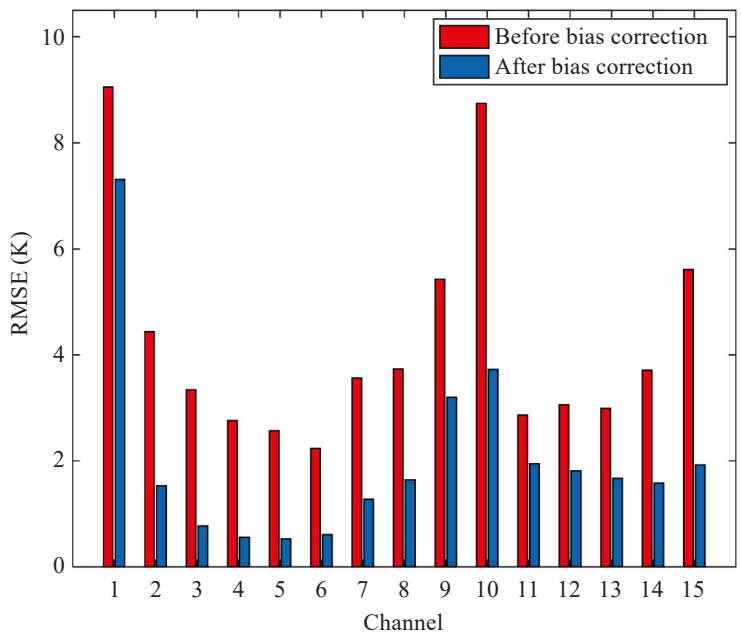

Figure 5. RMSEs between the observed brightness temperatures and the RTTOV-based simulated brightness temperatures before and after bias correction.

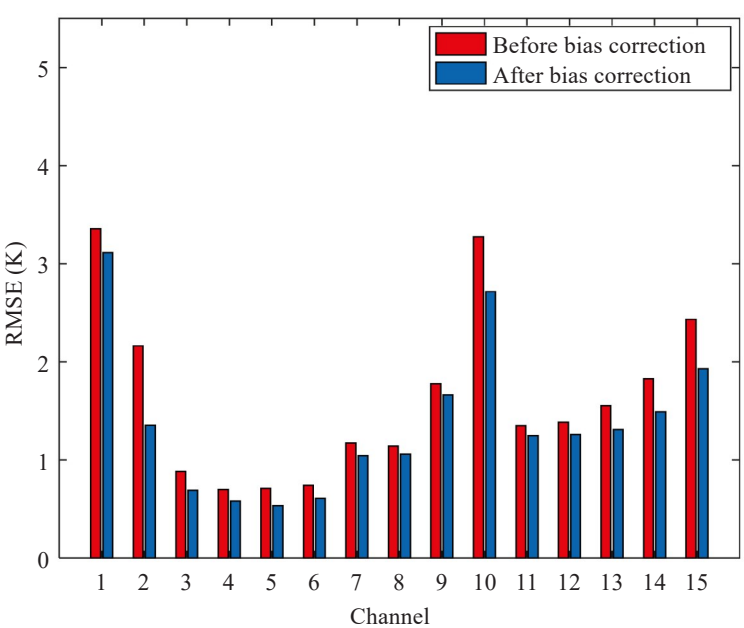

Figure 6. RMSEs between the observed brightness temperatures and the DNN-based simulated brightness temperatures before and after bias correction.

Table 2. RMSEs between the corrected brightness temperatures and the simulated brightness temperatures.

Channel	RTTOV-based (K)	DNN-based (K)	Channel	RTTOV-based (K)	DNN-based (K)
1	7.31	3.11	9	3.20	1.66
2	1.52	1.35	10	3.72	2.71
3	0.77	0.69	11	1.95	1.25
4	0.58	0.56	12	1.81	1.26
5	0.53	0.52	13	1.67	1.31
6	0.62	0.61	14	1.58	1.49
7	1.28	1.04	15	1.93	1.92
8	1.64	1.05			

As can be seen from Fig. 5, the bias correction method based on DNN developed in this study can be effectively performed to correct the RTTOV-based observation bias. RMSEs between the RTTOV-based corrected brightness temperatures and the RTTOV-based simulated brightness temperatures remain within 2 K for the temperature sounding channels 2-8, whose peak WF heights are distributed in the middle and upper atmosphere. For MWHTS window channels 1 and 10, and the temperature sounding channel 9, whose peak WF heights are close to the surface, although the corrections are significant, RMSEs between the RTTOV-based corrected brightness temperatures and the RTTOV-based simulated brightness temperatures are large, especially up to 7.3 K in channel 10. For humidity sounding channels 11-15, RMSEs between the RTTOV-based corrected brightness temperatures and the RTTOV-based simulated brightness temperatures all remain within 2 K. The magnitude of the bias correction being particularly noticeable in channel 15 is about 3.8 K.

It can be seen in Fig. 6 that although the bias correction method based on DNN can also be effectively performed for correcting the DNN-based observation bias, the correction is significantly less effective than that for the RTTOV-based observation bias as shown in Fig. 5. For MWHTS channels 2, 10, 14 and 15, the correction magnitudes are approximately 0.5 K, and the corrections for the remaining channels of MWHTS are not significant and the correction magnitudes are all within 0.3 K. However, it is important to note that in the 1DVAR algorithm, it is the RMSE between the corrected brightness temperature and the simulated brightness temperature that intrinsically affects the retrieval accuracy, rather than the correction magnitude for the observation bias.

Comparison of Fig. 5 and Fig. 6 shows that although the bias correction method based on DNN is much less effective in correcting the DNN-based observation bias than correcting the RTTOV-based observation bias, the RMSEs between the DNN-based corrected brightness temperatures and the DNN-based simulated brightness temperatures are smaller than the RMSEs between the RTTOV-based corrected brightness temperatures and the RTTOV-based simulated brightness temperatures in almost all channels of MWHTS, as can be seen in Table 2. Theoretically, the closer the corrected brightness temperatures are to the simulated brightness temperatures in the 1DVAR algorithm, the higher the retrieval accuracies of the temperature and humidity profiles using the corrected brightness temperatures. This can be validated by the 1DVAR retrieval system retrieving the temperature and humidity profiles using MWHTS observations.

6.3 *Retrieval results of the temperature and humidity profiles from MWHTS*

According to the design of Experiment 3 in Section 5, MWHTS observed brightness temperatures and the RTTOV-based corrected brightness temperatures in the retrieval testing dataset are input to the RTTOV-based 1DVAR retrieval system to obtain the retrieval results of the temperature and humidity profiles using the observed brightness temperatures before and after bias correction, respectively, and the retrieval accuracies are shown in Fig. 7. Similarly, MWHTS observed brightness temperatures and the DNN-based corrected brightness temperatures in the retrieval testing dataset are input to the DNN-based 1DVAR retrieval system to obtain the retrieval results of the temperature and humidity profiles using the observed brightness temperatures before and after bias correction, respectively, and the retrieval accuracies are shown in Fig. 8. Furthermore, the retrieval results from the RTTOV-based 1DVAR retrieval system and the DNN-based 1DVAR retrieval system are also concluded in Table 3 and Table 4, respectively, which are given at five different atmospheric levels corresponding to 100, 300, 500, 800, and 950 hPa for temperature and four levels for humidity except for the 100hPa level since the 100 hPa level is not reliable.

For the retrieval results of the temperature profiles from the RTTOV-based 1DVAR retrieval system, it can be seen from Fig. 7 that the retrieval accuracies of the RTTOV-based corrected brightness temperatures are significantly improved in the range of 250−1000 hPa compared to that of the observed brightness temperatures without bias correction, with the largest

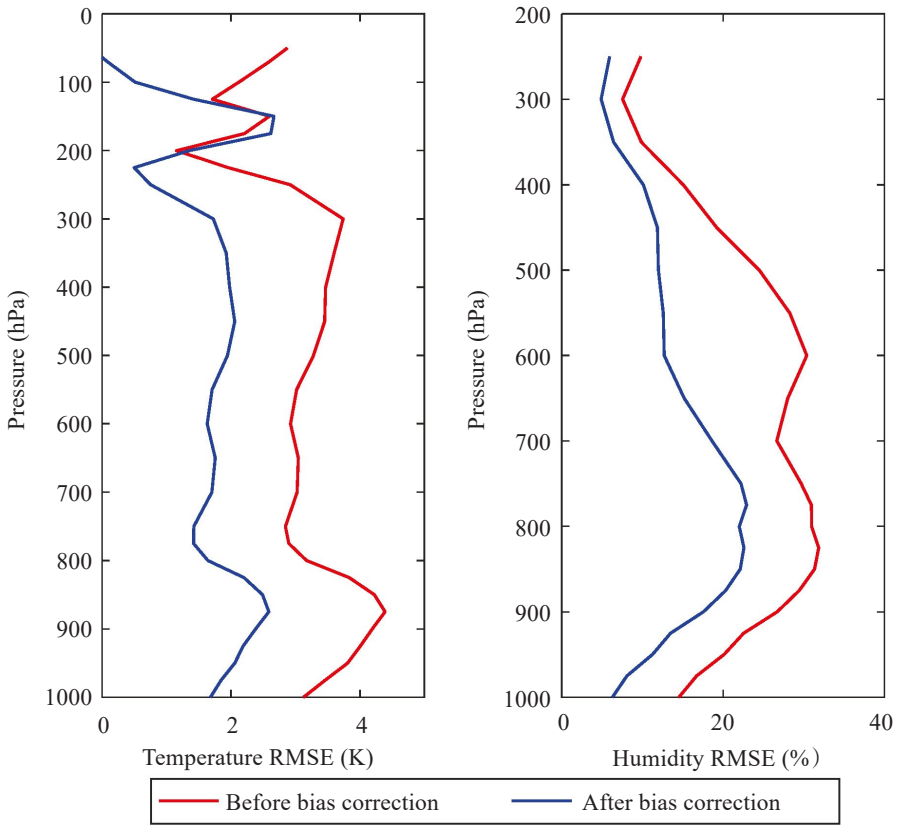

Figure 7. Retrieval accuracies of the temperature and humidity profiles from the RTTOV-based 1DVAR retrieval system.

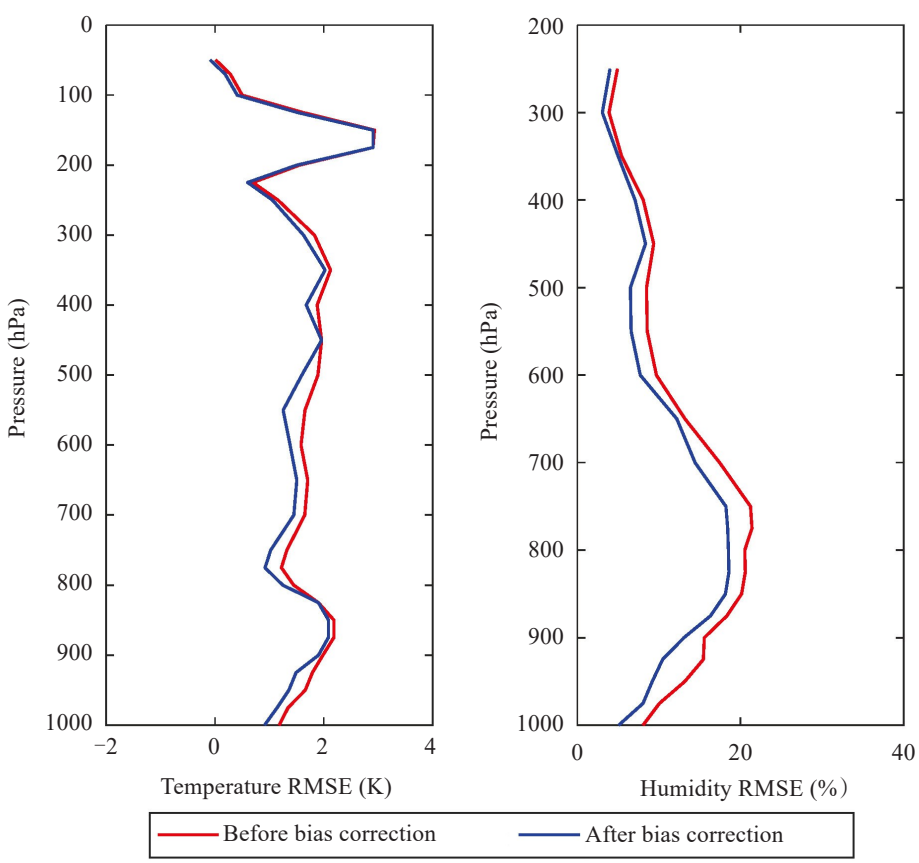

Figure 8. Retrieval accuracies of the temperature and humidity profiles from the DNN-based 1DVAR retrieval system.

Table 4. Summary of the retrieval accuracies of the RTTOV-based 1DVAR retrieval system.

	Observations		Corrected Observations	
Level (hPa)	Temperature RMSE (K)	Humidity RMSE (%)	Temperature RMSE (K)	Humidity RMSE (%)
100	2.12	–	0.52	–
300	3.74	7.53	1.73	4.85
500	3.28	24.47	1.94	11.97
800	3.17	30.96	1.64	22.01
950	3.81	20.14	2.06	11.26

Table 5. Summary of the retrieval accuracies of the DNN-based 1DVAR retrieval system.

	Observations		Corrected Observations	
Level (hPa)	Temperature RMSE (K)	Humidity RMSE (%)	Temperature RMSE (K)	Humidity RMSE (%)
100	0.51	–	0.40	–
300	1.83	3.86	1.62	3.05
500	1.91	8.47	1.58	6.51
800	1.44	20.50	1.25	18.43
950	1.66	13.16	1.35	9.21

improvements of about 2 K at 300 hPa and 900 hPa. The retrievals of the temperature profiles corresponding to the observed brightness temperatures before and after the bias correction are of comparable accuracy in the range of 125−200 hPa. For the retrieval results of the humidity profiles, the retrieval accuracies using the RTTOV-based corrected brightness temperatures are significantly improved at all atmospheric levels compared to that of the observed brightness temperatures without bias correction, with the largest improvement of about 15% at 600 hPa, and the improvements are about 9% in the range of 700−1000 hPa. Moreover, the retrieval accuracies of the temperature profile using the RTTOV-based corrected brightness temperatures are within approximately 3K in the range of 200−1000 hPa, and the retrieval accuracies of the humidity profile using the RTTOV-based corrected brightness temperatures are within 22% at all atmospheric levels.

For the retrieval results of the temperature profile from the DNN-based 1DVAR retrieval system, it can be seen from Fig. 8 that the retrieval accuracies using the DNN-based corrected brightness temperatures are not greatly improved compared to the observed brightness temperatures without bias correction, with the largest improvement being approximately 0.4 K at 550 hPa. For the retrieval results of the humidity profile, the retrieval accuracies of the DNN-based corrected brightness temperatures are also not significantly improved compared to the observed brightness temperatures without bias correction, with the largest improvement at 1000 hPa being about 3%. Furthermore, the retrieval accuracies of the temperature profile using the DNN-based corrected brightness temperatures are within approximately 2.5 K in the range of 200−1000 hPa, and the retrieval accuracies of the humidity profile using the DNN-based corrected brightness temperatures are within 18.5% at all atmospheric levels.

The comparison of the retrieval results of the RTTOV-based 1DVAR retrieval system and the DNN-based 1DVAR retrieval system shows that the observation bias correction can improve the retrieval accuracies of the RTTOV-based 1DVAR retrieval system more significantly. However, comparison of Fig. 7 and Fig. 8 unveils that both the temperature retrieval accuracy and the humidity retrieval accuracy using the DNN-based corrected brightness temperatures improve at all atmospheric levels compared to that of the RTTOV-based corrected brightness temperatures, with the greatest improvement in temperature and humidity retrieval accuracies at 1000 hPa of approximately 0.8 K and 600 hPa of about 7%, respectively. Furthermore, for the retrieval results using the corrected brightness temperatures, a comparison of Table 4 and Table 5 shows that the improvements in the temperature retrieval accuracies of the DNN-based 1DVAR retrieval system compared to that of the RTTOV-based 1DVAR retrieval system at 100 hPa, 300 hPa, 500 hPa, 800 hPa, and 950 hPa are 0.12 K, 0.11 K, 0.36 K, 0.39 K, and 0.71 K, respectively. The improvements in humidity retrieval accuracies are 1.8%, 5.5%, 3.6%, and 2% at 300 hPa, 500 hPa, 800 hPa, and 950 hPa, respectively. The reason why the DNN-based 1DVAR retrieval system can improve the retrieval accuracies compared to the

RTTOV-based 1DVAR retrieval system for the temperature and humidity profiles is that the DNN-based radiative transfer model applied to the 1DVAR algorithm can obtain higher accuracies than RTTOV for the simulated brightness temperatures, the corrected brightness temperatures in the iterative solution process are closer to the simulated brightness temperatures, and the solved temperature and humidity profiles are closer to the true values.

In summary, the comparison of the bias correction results for the MWHTS observations and the comparison of the retrieval results of the 1DVAR algorithm before and after the observation bias correction shows that the better the observation bias correction, the more obvious the improvement in the retrieval accuracy. And the closer the brightness temperatures input to the 1DVAR algorithm are to the simulated brightness temperatures generated by the radiative transfer model in the 1DVAR algorithm, the better the retrieval accuracy of the 1DVAR algorithm. It can also be concluded that the DNN-based radiative transfer model applied to the 1DVAR algorithm can improve the performance of the 1DAVR algorithm because of the higher accuracy in simulating the brightness temperature that can be obtained.

7 CONCLUSION

In this study, DNN is used to describe the relationship between the atmospheric parameters and MWHTS observations, and the DNN-based radiative transfer model is developed. Compared to the traditional operational radiative transfer model RTTOV, the DNN-based radiative transfer model can obtain higher accuracies in simulating MWHTS observations for all 15 channels of MWHTS. When the DNN-based radiative transfer model and RTTOV to the 1DVAR algorithm are applied, the DNN-based 1DVAR retrieval system and the RTTOV-based 1DVAR retrieval system can be built respectively. Compared to the RTTOV-based 1DVAR retrieval system, the DNN-based 1DVAR retrieval system can achieve higher retrieval accuracies of the temperature and humidity profiles using MWHTS measurements. The DNN-based radiative transfer model and the DNN-based 1DVAR retrieval system developed in this study are important references for both the forward and retrieval problems in the microwave remote sensing of atmospheric parameters.

However, although the DNN-based radiative transfer model developed in this study is successfully applied to the 1DVAR algorithm, the accuracy of the DNN-based radiative transfer model is affected by the weather conditions, which is similar to the physical-based radiative transfer model, and thus shows different performance in retrieving atmospheric parameters. Therefore, building DNN-based radiative transfer models according to different weather conditions is our next research focus. However, it should be noted that how to classify satellite data according to different weather conditions based on the characteristics of satellite data is the key to realize applications of satellite data. Moreover, the developed DNN-based radiative transfer model in this study cannot consider gas absorption, transmissivity, surface emissivity, Jacobians, etc., compared with the physical-based radiative transfer model, so further research on the DNN-based radiative transfer model is needed to expand its application in the field of atmospheric science.

***Acknowledgments*:** The authors would like to thank NSMC for providing the MWHTS observations, as well as ECMWF for providing the ERA-Interim reanalysis data.

REFERENCES

[1] TURNER D D, LÖHNERT U. Ground-based temperature, and humidity profiling: Combining active and passive remote sensors [J]. Atmospheric Measurement Techniques, 2021, 14(4): 3033-3048, https://doi. org / 10.5194 / amt-14-3033-2021

[2] ZHANG L, YIN X, WANG Z, et al. Preliminary analysis of the potential and limitations of MICAP for the retrieval of sea surface salinity [J]. IEEE Journal of Selected Topics in Applied Earth Observations and Remote Sensing, 2018, 11 (9): 2979-2990, https://doi. org / 10.1109 / JSTARS.2018.2849408

[3] EBELL K, LÖHNERT U, PÄSCHKE E, et al. A 1 - D variational retrieval of temperature, humidity, and liquid cloud properties: Performance under idealized and real conditions [J]. Journal Geophysical Research: Atmospheres, 2017, 122(3): 1746-1766, https://doi. org / 10.1002/2016JD025945

[4] ZHANG R, KUMMEROW C, RANDEL D, et al. Tropical cyclone rain retrievals from FY-3B MWRI brightness temperatures using the goddard profiling algorithm (GPROF) [J]. Journal of Atmospheric and Oceanic Technology, 2019, 36(5): 849-864, http://doi. org / 10.1175 / JTECH-D-18-0167.1

[5] LI N, HE J, ZHANG S, et al. Precipitation retrieval using 118.75 GHz and 183.31 GHz channels from MWHTS on FY-3C satellite [J]. IEEE Journal of Selected Topics in Applied Earth Observations and Remote Sensing, 2018, 11 (11): 4373-4389, http://doi. org / 10.1109 / JSTARS.2018.2873255

[6] EBELL K, ORLANDI E, HÜNERBEIN A, et al. Combining ground-based with satellite-based measurements in the atmospheric state retrieval: assessment of the information content [J]. Journal Geophysical Research: Atmospheres, 2013, 118(13): 6940-6956, https://doi.org/10.1002/jgrd.50548

[7] POLYAKOV A, TIMOFEYEV Y M, VIROLAINEN Y. Comparison of different techniques in atmospheric temperature-humidity sensing from space [J]. International Journal of Remote Sensing, 2014, 35(15): 5899-5912, https://doi.org/10.1080/01431161.2014.945004

[8] TAN H, MAO J, CHEN H, et al. A study of a retrieval method for temperature and humidity profiles from microwave radiometer observations based on principle component analysis and stepwise regression [J]. Journal of

Atmospheric and Oceanic Technology, 2011, 28(3): 378-389, https://doi.org/10.1175/2010JTECHA1479.1

[9] GOHIL B S, GAIROLA R M, MATHUR A K, et al. Algorithms for retrieving geophysical parameters from the MADRAS and SAPHIR sensors of the Megha-Tropiques satellite: Indian scenario [J]. Quarterly Journal of the Royal Meteorological Society, 2013, 139(673): 954-963, https://doi.org/10.1002/qj.2041

[10] CHAKRABORTY R, MAITRA A. Retrieval of atmospheric properties with radiometric measurements using neural network [J]. Atmospheric Research, 2016, 181: 124-132, https://doi. org / 10.1016 / j. atmosres.2016.05.011

[11] HE Q, WANG Z, LI J. Application of the deep neural network in retrieving the atmospheric temperature and humidity profiles from the microwave humidity and temperature sounder onboard the Feng-Yun-3 satellite [J]. Sensors, 2021, 21(14): 4673, https://doi. org / 10.3390 / s21144673

[12] HE J, ZHANG S, WANG Z. The retrievals and analysis of clear-sky water vapor density in the Arctic regions from MWHS measurements on FY-3A satellite [J]. Radio Science, 2012, 47(2): RS2009, https://doi. org / 10.1029 / 2010RS004612

[13] LIU Q, WENG F. One-dimensional variational retrieval algorithm of temperature, water vapor, and cloud water profiles from advanced microwave sounding unit (AMSU) [J]. IEEE Transactions on Geoscience and Remote Sensing, 2005, 43(5): 1087-1095, https://doi.org/10.1109/TGRS.2004.843211

[14] AIRES F, PRIGENT C, ORLANDI E, et al. Microwave hyper-spectral measurements for temperature and humidity atmospheric profiling from satellite: the clear-sky case [J]. Journal Geophysical Research: Atmospheres, 2015, 120(21): 11334-11351, https://doi. org / 10.1002 / 2015JD023331

[15] BOUKABARA S A, GARRETT K, CHEN W, et al. MiRS: An all-weather 1DVAR satellite data assimilation and retrieval system [J]. IEEE Transactions on Geoscience and Remote Sensing, 2011, 49(9): 3249-3272, https://doi.org/10.1109/TGRS.2011.2158438

[16] HE Q R, WANG Z Z, HE J Y, et al. A comparison of the retrieval of atmospheric temperature profiles using observations of the 60 GHz and 118.75 GHz absorption lines [J]. Journal of Tropical Meteorology, 2018, 24(2): 151-162, https://doi. org / 10.16555 / j. 1006-8775.2018.02.004

[17] BLACKWELL W J, CHEN F W. Neural Networks in Atmospheric Remote Sensing [M]. Norwood: Artech House Press, 2009: 19-32.

[18] HE Q, WANG Z, LI J. Fusion retrieval of sea surface barometric pressure from the microwave humidity and temperature sounder and microwave temperature Sounder-II onboard the Fengyun-3 satellite [J]. Remote Sensing, 2022, 14(2): 276, https://doi.org/10.3390/rs14020276

[19] ROSENKRANZ P W. Retrieval of temperature and moisture profiles from AMSU-A and AMSU-B measurements [J]. IEEE Transactions on Geoscience and Remote Sensing, 2001, 39(11): 2429-2435, https://doi.org/10.1109/36.964979

[20] ISHIMOTO H, OKAMOTO K, OKAMOTO H, et al. One-dimensional variational (1D-Var) retrieval of middle to upper tropospheric humidity using AIRS radiance data [J]. Journal Geophysical Research: Atmospheres, 2014, 119(12): 7633-7645, https://doi. org / 10.1002 / 2014JD021706

[21] RODGERS C D. Inverse Methods for Atmospheric Sounding: Theory and Practice [M]. Hackensack & London: World Scientific Press, 2000: 67-75.

[22] SUSSKIND J, ROSENFIELD J, REUTER D. An accurate radiative transfer model for use in the direct physical inversion of HIRS2 and MSU temperature sounding data [J]. Journal Geophysical Research: Oceans, 1983, 88 (C13): 8550-8568, https://doi. org / 10.1029 / JC088iC13p08550

[23] SAUNDERS R, HOCKING J, TURNER E, et al. An update on the RTTOV fast radiative transfer model (currently at version 12) [J]. Geoscientific Model Development, 2018, 11(7): 2717-2737, https://doi. org / 10.5194/gmd-11-2717-2018

[24] LIU Q, BOUKABARA S. Community radiative transfer model (CRTM) applications in supporting the Suomi National Polar-orbiting Partnership (SNPP) mission validation and verification [J]. Remote Sensing of Environment, 2014, 140: 744-754, https://doi.org/10.1016/j.rse.2013.10.011

[25] BUEHLER S A, ERIKSSON P, KUHN T, et al. ARTS, the atmospheric radiative transfer simulator [J]. Journal of Quantitative Spectroscopy and Radiative Transfer, 2005, 91(1): 65-93, https://doi.org/10.1016/j.jqsrt.2004.05.051

[26] ERIKSSON P, BUEHLER S A, DAVIS C P, et al. ARTS, the atmospheric radiative transfer simulator, version 2 [J]. Journal of Quantitative Spectroscopy and Radiative Transfer, 2011, 112(10): 1551-1558, https://doi. org / 10.1016/j.jqsrt.2011.03.001

[27] ELACHI C, ZYL J V. Introduction to the Physics and Techniques of Remote Sensing [M]. Hoboken: John Wiley & Sons Inc Press, 2006: 385-412.

[28] YAN X, LIANG C, JIANG Y, et al. A deep learning approach to improve the retrieval of temperature and humidity profiles from a ground-based microwave radiometer [J]. IEEE Transactions on Geoscience and Remote Sensing, 2020, 58(12): 8427-8437, https://doi.org/10.1109/TGRS.2020.2987896

[29] GUO Y, LU N M, QI C L, et al. Calibration and validation of microwave humidity and temperature sounder onboard FY-3C satellite [J]. Chinese Journal of Geophysics (in Chinese), 2015, 58(1): 20-31, https://doi / 10.6038 / cjg20150103

[30] WANG Z, LI J, HE J, et al. Performance analysis of microwave humidity and temperature sounder onboard the FY-3D satellite from prelaunch multiangle calibration data in thermal / vacuum test [J]. IEEE Transactions on Geoscience and Remote Sensing, 2019, 57(3): 1664-1683, https://doi/10.1109/TGRS.2018.2868324

[31] HE Q R, WANG Z Z, HE J Y, et al. Effects of a cloud filtering method for Fengyun-3C microwave humidity and temperature sounder measurements over ocean on retrievals of temperature and humidity [J]. Journal of Tropical Meteorology, 2018, 24(1): 29-41, https://doi / 10.16555/j.1006-8775.2018.01.003

[32] CARMINATI F, MIGLIORINI S. All-sky data assimilation of MWTS-2 and MWHS-2 in the Met Office global NWP system [J]. Advances Atmospheric Sciences,

2021, 38(10): 1682-1694, https://doi.org/10.1007/s00376-021-1071-5

[33] DEE D P, UPPALA S M, SIMMONS A J, et al. The ERA-Interim reanalysis: configuration and performance of the data assimilation system [J]. Quarterly Journal of the Royal Meteorological Society, 2011, 137(656): 553-597, https://doi.org/10.1002/qj.828

[34] ULABY F T, MOORE R K, FUNG A K. Microwave Remote Sensing: Active and Passive [M]. Norwood: Artech House Press, 1981: 121-145.

[35] ZHOU Y, GRASSTOTTI C. Development of a machine learning-based radiometric bias correction for NOAA's microwave integrated retrieval system (MiRS) [J]. Remote Sensing, 2020, 12(19): 3160, https://doi. org / 10.3390/rs12193160

[36] LI Q, WEI M, WANG Z, et al. Improving the retrieval of cloudy atmospheric profiles from brightness temperatures observed with a ground-based microwave radiometer [J]. Atmosphere, 2021, 12(5): 648, https://doi. org / 10.3390 / atmos12050648

[37] TAN J, NOURELDEEN N, MAO K, et al. Deep learning convolutional neural network for the retrieval of land surface temperature from AMSR2 data in China [J]. Sensors, 2019, 19(13): 2987, https://doi. org / 10.3390 / s19132987

[38] RODGERS C D. Retrieval of atmospheric temperature and composition from remote measurements of thermal radiation [J]. Reviews of Geophysics and Space Physics, 1976, 14(4): 609-624, https://doi. org / 10.1029 / RG014i004p00609

[39] LECUN Y, BENGIO Y, HINTON G. Deep learning [J]. Nature, 2015, 521: 436-444, https://doi. org / 10.1038 / nature14539

[40] LEE Y, HAN D, AHN M H, et al. Retrieval of total precipitable water from Himawari-8 AHI data: a comparison of random forest, extreme gradient boosting, and deep neural network [J]. Remote Sensing, 2019, 11 (15): 1741, https://doi.org/10.3390/rs11151741

[41] SRIVASTAVA N, HINTON G, KRIZHEVSKY A, et al. Dropout: a simple way to prevent neural networks from overfitting [J]. Journal of Machine Learning Research, 2014, 15(1): 1929-1958

[42] SAHOO S, BOSCH-LLUIS X, REISING S C, et al. Optimization of background information and layer thickness for improved accuracy of water-vapor profile retrieval from ground-based microwave radiometer measurements at *k*-band [J]. IEEE Journal of Selected Topics in Applied Earth Observations and Remote Sensing, 2015, 8(9): 4284-4295, https://doi. org / 10.1109 / JSTARS.2014.2370073

[43] DEE D P. Bias and data assimilation [J]. Quarterly Journal of the Royal Meteorological Society, 2005, 131(613): 3323-3343, https://doi.org/10.1256/qj.05.137

[44] AULIGNE T, MCNALLY A P, DEE D P. Adaptive bias correction for satellite data in a numerical weather prediction system [J]. Quarterly Journal of the Royal Meteorological Society, 2007, 133(624): 631-642, https://doi.org/10.1002/qj.56

[45] GAYFULIN D, TSYRULNIKOV M, USPENSKY A, et al. Assessment and adaptive correction of observations in atmospheric sounding channels of the satellite microwave radiometer MTVZA-GY [J]. Pure and Applied Geophysics, 2018, 175(10): 3653-3670, https://doi. org / 10.1007/s00024-018-1917-7

[46] KAZUMORI M. Satellite radiance assimilation in the JMA operational mesoscale 4DVAR system [J]. Monthly Weather Review, 2014, 142(3): 1361-1381, https://doi.org/10.1175/MWR-D-13-00135.1

[47] ZHU Y, DERBER J, COLLARD A, et al. Enhanced radiance bias correction in the national centers for environmental prediction's gridpoint statistical interpolation data assimilation system [J]. Quarterly Journal of the Royal Meteorological Society, 2014, 140 (682): 1479-1492, https://doi.org/10.1002/qj.2233

[48] DEE D P, UPPALA S. Variational bias correction of satellite radiance data in the ERA-Interim reanalysis [J]. Quarterly Journal of the Royal Meteorological Society, 2009, 135(644): 1830-1841, https://doi.org/10.1002/qj.493

[49] HE Q, WANG Z, HE J. Bias correction for retrieval of atmospheric parameters from the Microwave Humidity and Temperature Sounder onboard the Fengyun-3C satellite [J]. Atmosphere, 2016, 7(12): 156, https://doi.org/10.3390/atmos7120156

[50] LÖHNERT U, CREWELL S, SIMMER C. An integrated approach toward retrieving physically consistent profiles of temperature, humidity, and cloud liquid water [J]. Journal of Applied Meteorology, 2004, 43(9): 1295-1307, https://doi. org / 10.1175 / 1520-0450(2004)043<1295: AIATRP>2.0.CO;2

Citation: HE Qiu-rui, ZHANG Rui-ling, LI Jiao-yang, et al. Research on the Application of the Radiative Transfer Model Based on Deep Neural Network in One-dimensional Variational Algorithm [J]. Journal of Tropical Meteorology, 2022, 28(3): 326-342, https://doi.org/10.46267/j.1006-8775.2022.025